crystals

Article

Enhanced Broadband Metamaterial Absorber Using Plasmonic Nanorods and Muti-Dielectric Layers Based on ZnO Substrate in the Frequency Range from 100 GHz to 1000 GHz

Ahmed Emara [1,2,*], Amr Yousef [1,2], Basma ElZein [1,3], Ghassan Jabbour [4] and Ali Elrashidi [1,2]

1 Department of Electrical Engineering, University of Business and Technology, Jeddah 21432, Saudi Arabia
2 Department of Engineering Physics, Alexandria University, Alexandria 21544, Egypt
3 Sustainable Development, Global Council for Tolerance and Peace, VLT1011 Valletta, Malta
4 Advanced Materials and Devices Laboratories, University of Ottawa, 75 Laurier Ave. E, Ottawa, ON K1N 6N5, Canada
* Correspondence: a.emara@ubt.edu.sa

Abstract: A broadband thin film plasmonic metamaterial absorber nanostructure that operates in the frequency range from 100 GHz to 1000 GHz is introduced and analyzed in this paper. The structure consists of three layers: a 200 nm thick gold layer that represents the ground plate (back reflector), a dielectric substrate, and an array of metallic nanorods. A parametric study is conducted to optimize the structure based on its absorption property using different materials, gold (Au), aluminum (Al), and combined Au, and Al for the nanorods. The effect of different dielectric substrates on the absorption is examined using silicon dioxide (SiO_2), aluminum oxide (Al_2O_3), titanium dioxide (TiO_2), and a combination of these three materials. This was followed by the analysis of the effect of the distribution of Al, and Au nanorods and their dimensions on the absorption. The zinc oxide (ZnO) layer is added as a substrate on top of the Au layer to enhance the absorption in the microwave range. The optimized structure achieved more than 80% absorption in the ranges 100–280 GHz, 530–740 GHz and 800–1000 GHz. The minimum optimized absorption is more than 65% in the range 100 GHz to 1000 GHz.

Keywords: electromagnetic absorbers; metamaterial absorbers; SiO_2; Al_2O_3; TiO_2; ZnO; microwave absorbers; plasmonic metamaterial absorbers; absorption spectrum; FDTD

check for updates

Citation: Emara, A.; Yousef, A.; ElZein, B.; Jabbour, G.; Elrashidi, A. Enhanced Broadband Metamaterial Absorber Using Plasmonic Nanorods and Muti-Dielectric Layers Based on ZnO Substrate in the Frequency Range from 100 GHz to 1000 GHz. *Crystals* **2022**, *12*, 1334. https://doi.org/10.3390/cryst12101334

Academic Editor: George Kenanakis

Received: 30 August 2022
Accepted: 18 September 2022
Published: 21 September 2022

1. Introduction

Recently, electromagnetic wave absorbers (EMAs) have attracted researchers' intertest due to their varied applications in the field of energy harvesting, avion stealth, sensing as well as suppressing the increasing electromagnetic radiations from electronic devices everywhere around us.

Classical EMAs depend on multireflection and interference of electromagnetic waves and could be divided into three types: Salisbury absorbers, Jaumann absorbers, and circuit analog absorbers. Salisbury absorbers consist of a metal plate separated from a resistive sheet by a dielectric material of a quarter wavelength thickness [1–3]. The interference between the reflected wave from the bottom metal plate and the upper resistive sheet is destructive and hence, the EM wave is trapped, and the energy is dissipated in the resistive sheet. Jaumann absorbers use the same concept as the Salisbury absorbers, but Jaumann absorbers use more than one resistive sheet to broaden the absorption bandwidth (BW) of the device [4,5]. The analog circuit absorbers' design is the same as Salisbury absorbers' design but with the top resistive sheet replaced by a periodic top metallic reactive surface that makes the analog circuit absorbers frequency selective absorbers [6,7]. The main disadvantage of the three types of classical absorbers is the need of a dielectric material of quarter wavelength thickness that makes the absorbing device bulky, with limited design flexibility which in turn limits its applicability.

To overcome the drawbacks of classical EMAs, researchers focused on developing new absorbers with thin thickness, light weight, and tunable absorption. In 2008, the first perfect metamaterial absorber (MMA) was proposed by Landy. The unit cell of Landy's absorber consists of two standard split ring resonators connected by an inductive ring parallel to the split wire with a thin dielectric material between them [8]. Generally, MMAs consist of three main layers: ground metal plane, dielectric substrate, and a top metallic periodic patch. The thickness of dielectric layer can be tailored to be much less than the wavelength of the incident electromagnetic wave. Research in the field of EMAs has been accelerated after Landy's perfect absorber due to the prospective applications of the EMAs such as solar energy harvesting, stealth, biological sensors, refractive index sensors, photodetection, photovoltaic devices, and optical switches [9–17].

EMAs can be structured to absorb EM waves in the spectrum range from microwave to visible region. Y. Cheng et al. have reported a metamaterial absorber composed of a single closed-meander-wire resonator structure placed over a metal ground plane separated by a dielectric substrate. They obtained about 90% absorption at different resonance frequencies in the range from 4 to 12 GHz, but this MMA is not suitable for wide bandwidth applications [18]. Using a periodic array of indium tin oxide (ITO) film sandwiched between two polyvinyl chloride layers, Q. Zhou et al. have designed a metamaterial microwave absorber that achieved 90% absorption in the narrow range from 8 to 18 GHz [19]. S. Lai et al. have proposed an MMA with ITO as the top resonance structure array layer, glass as the medium layer, and another ITO as the bottom ground layer. They achieved more than 80% absorption from 15.6 to 39 GHz [20]. J. Ning et al. designed an MMA that operates in the range from 0.4 to 1 GHz with 90% absorption as well, using magnetic nanomaterial and a varactor [21]. Md. Hossain has reported 99.7% to 99.9% EM wave absorption at triple frequencies 5.37, 10.32, and 12.25 GHz using MMA consisting of two split ring copper resonators separated by a dielectric layer [22]. All of these microwave MMAs have a very narrow bandwidth and operate over a narrow range of frequencies.

Recently, thin film MMAs use localized surface plasmon polaritons (LSPPs) to realize small size thin absorber in visible, infrared, and terahertz ranges of the spectrum. W. guo et al. reported infrared MMA using two gold (Au) metallic layers and ZnS dielectric layer sandwiched between them. They got absorption that exceeded 90% in the range from 7.8 to 12.1 μm. The absorption range is enlarged (5.3 to 13.7 μm) by using double Au-ZnS-Au layers on the top of each other but with only 80% absorption [23]. Terahertz plasmonic MMA is reported by Y. Kang et al. using an Au substrate followed by a dielectric material of a dielectric constant of 1.96, with an Au cylinder on the top of the dielectric layer. They obtained two 99% absorption peaks at 275 and 440 THz [24]. Using a ground Au plate, and an array of Au resonators on top of silicon dioxide (SiO_2) substrate, D. Katrodiya et al. have achieved metamaterial broadband solar absorber with an average of 89.79% absorption in the frequency range from 155 to 1595 THz [25]. These reported plasmonic MMAs showed high performance in the infrared and terahertz ranges but suffer from degraded performance in the microwave range.

There is an interest in ZnO driven by its prospects in optoelectronics applications owing to its unique properties such as direct wide band gap Eg~3.3 eV at 300 K. It has been widely known as a versatile material for its different applications in the production of green, blue-ultraviolet, and white light-emitting devices, electronics, and optoelectronics devices. Furthermore, ZnO is known for its strong luminescence in the green–white region of the spectrum, strong sensitivity of surface conductivity to the presence of adsorbed species, and high thermal conductivity. The n-type conductivity of ZnO makes it appropriate for different applications such as metamaterial absorbers [26,27]. On the other hand, SiO_2 is a material of considerable technological importance due to its wide applications in electronics and optoelectronics devices, with a very wide bandgap of 9.6 eV [28]. TiO_2, has been widely investigated in environmental and energy research, due to its wide bandgap of 3.2 eV, which allows it to absorb the UV light [29]. The combination of these materials will play a vital role in affecting the impedance of the proposed metamaterial absorber.

In this work, we introduced an enhanced broadband thin film plasmonic MMA that operates in the frequency range from 100 to 1000 GHz. An absorption above 80% is obtained in the range from 700 to 1000 GHz, while it fluctuates between 60% and 80% in the range below 700 GHz. This proposed absorber is found to be insensitive to light polarization and the direction of incident light. The paper is organized as follows: first, the proposed design of the plasmonic MMA is presented; then the simulation results are illustrated and discussed which yields to an optimized MMA design. Finally, the conclusion summarizes the process and the results of this research.

2. Proposed Structure Design and Its Operation Principle

The typical thin film MMA structure has been adopted in this research, which consists of three layers: a metallic Au ground square plate of 200 nm thickness and cross section area of 1×10^4 nm^2, a 4×4 array of metallic equally spaced nanorods of height h = 50 nm and radius r = 60 nm, and a dielectric substrate of height h_1 = 60 nm sandwiched between the ground plate and the metallic rods. The schematic diagram of the adopted structure is shown in Figure 1. The gold ground plate acts as a back reflector layer that is used to enhance light trapping and reflects the transmitted light to the structure for more light absorption [30,31]. The spacing (X) between any two successive nanorods could be calculated as:

$$\mathbf{X} = \frac{\mathbf{L}}{\mathbf{4}} - \mathbf{2r} \tag{1}$$

where L is the side length of the square ground metallic plate, and r is the radius of the nanorod. The distance between the center of the outer rod and the edge of the unit cell is assumed X/2.

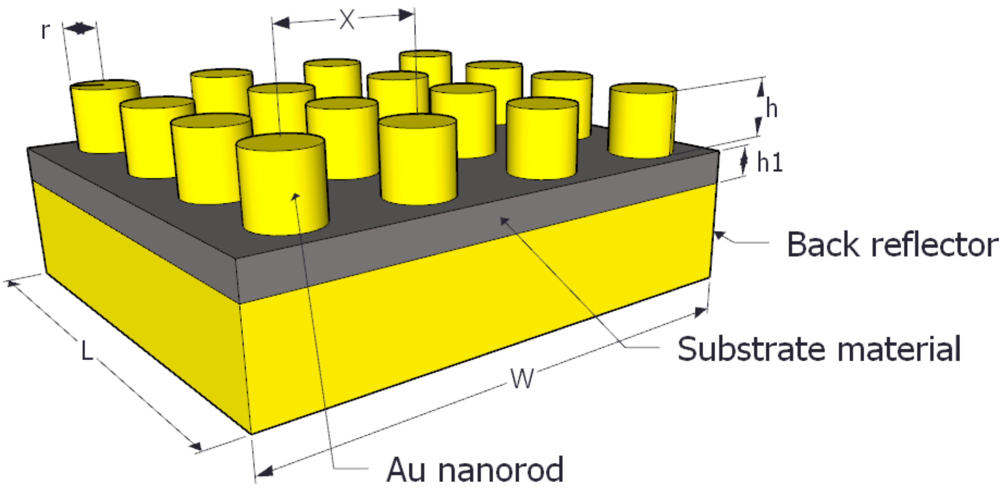

Figure 1. Schematic diagram of the adopted typical MMA structure.

The principle of operation of MMAs depends on resonance. When an electromagnetic wave at a resonance frequency coincides on the MMA, a pair of anti-parallel oscillating currents are induced in the ground metallic layer and the upper metallic nanorods so, a magnetic resonance is established. Moreover, local surface plasmons are generated at the resonance wavelength, and electric resonance is established between the ground metallic layer and the nanorods. Absorption is a result of this resonance, as the electromagnetic wave will be confined in the MMA unit cell and electromagnetic power at the resonance frequency is consumed due to losses in the metallic layer and dielectric layer [8,32,33]. Absorptance (A(f)) of the MMA could be calculated from the relation [34]:

$$\mathbf{A(f) = 1 - R(f) - T(f)} \tag{2}$$

where R(f) and T(f) are the reflectance and transmittance of the absorber, respectively. The reflectance and transmittance could be calculated from the reflection coefficient (S_{11}), and transmission coefficient (S_{21}):

$$\mathbf{R(f) = |S_{11}|^2} \tag{3}$$

$$\mathbf{T(f) = |S_{21}|^2} \tag{4}$$

Due to the back reflector metallic ground layer, the transmission coefficient is zero and hence, the absorptance A(f) is given by:

$$\mathbf{A(f) = 1 - |S_{11}|^2} \tag{5}$$

The absorptance depends on the input impedance of the MMA structure, and is given by [20]:

$$\mathbf{A(f) = 1 - \left| \frac{Z_{in}(f) - Z_o}{Z_{in}(f) + Z_o} \right|} \tag{6}$$

where Z_{in} is the input impedance of the MMA structure, and Z_0 = 377 Ω is the free space impedance. At resonance, the input impedance is matched to the free space impedance, so perfect absorption occurs at the resonance frequency.

Plasmonic nanorods distributed on the substrate layer change the absorbed optical power inside the proposed structure, the absorption depends on the maximum reflectivity. Nanorod shape and size are the main parameters that affect the absorbed optical power in addition to the relative permittivity of the plasmonic nanorods and dielectric constant of the surrounding medium [35]. The maximum absorption occurred at the wavelength known as λ_{max}, the maximum peak of the wavelength, which can be calculated using Equation (7).

$$\boldsymbol{\lambda_{max} = \frac{P}{n} \left(\frac{\varepsilon_n \varepsilon_m(\lambda_{max})}{\varepsilon_m + \varepsilon_n(\lambda_{max})} \right)^{1/2}} \tag{7}$$

where (ε_m) is the permittivity of the surrounding medium, (ε_n) is the plasmonic nanorod dielectric constant at corresponding (λ_{max}), (n) is an integer and (P) is the periodicity of the structural.

Hence, the plasmonic nanorod dielectric permittivity can be calculated using a multi-oscillator Drude-Lorentz model [35] as shown in Equation (8):

$$\boldsymbol{\varepsilon_n = \varepsilon_\infty - \frac{\omega_D^2}{\omega^2 + j\omega\gamma_D} - \sum_{Y=1}^{6} \frac{\delta_k \omega_k^2}{\omega^2 - \omega_k^2 + 2j\omega\gamma_k}} \tag{8}$$

where (ε_∞) is the nanorod high-frequency dielectric permittivity, (ω_D) is the plasma frequency of the free electrons, (γ_D) is the collision frequency of the free electrons, (δ_k) is the amplitude of Lorentz oscillator, (ω_k) is the resonance angular frequencies and (γ_k) is the damping constants for (Y) value from 1 to 6.

To calculate the absorbed power, the refractive indexes of all used material are given as follows; TiO_2 follows the Devore model [36], however, the value for silicon dioxide is a function of the wavelength and follows Aspnes and Studna model [37], and the refractive index of zinc oxide is considered as given by Kaur et al. [38]. On the other hand, the refractive index of different plasmonic materials is summarized using Equation (8) in Table 1 [39]. The dielectric constants of the used materials are shown in Figures A1–A4 in Appendix A.

Table 1. Plasmonic parameters which are used for the metallic materials.

Material	Term	Strength	Plasma Frequency	Resonant Frequency	Damping Frequency
Au	0	0.7600	0.137188×10^{17}	0.000000×10^{0}	0.805202×10^{14}
	1	0.0240	0.137188×10^{17}	0.630488×10^{15}	0.366139×10^{15}
	2	0.0100	0.137188×10^{17}	0.126098×10^{16}	0.524141×10^{15}
	3	0.0710	0.137188×10^{17}	0.451065×10^{16}	0.132175×10^{16}
	4	0.6010	0.137188×10^{17}	0.653885×10^{16}	0.378901×10^{16}
	5	4.3840	0.137188×10^{17}	0.202364×10^{17}	0.336362×10^{16}
Al	0	0.5230	0.227583×10^{17}	0.000000×10^{0}	0.714047×10^{14}
	1	0.2270	0.227583×10^{17}	0.246118×10^{15}	0.505910×10^{15}
	2	0.0500	0.227583×10^{17}	0.234572×10^{16}	0.474006×10^{15}
	3	0.1660	0.227583×10^{17}	0.274680×10^{16}	0.205251×10^{16}
	4	0.0300	0.227583×10^{17}	0.527635×10^{16}	0.513810×10^{16}

The proposed structure is analyzed and optimized using an electromagnetic wave solver, Lumerical Finite Difference Time Domain (FDTD) solutions software. In the simulation of a unit cell, the boundary conditions are considered as a periodic structure in x and y directions, and the layers are perfectly matched in z-direction. A plane wave source with a frequency band 100–1000 GHz is used as a light source, and the minimum mesh size is 0.5 nm in all directions with an offset time of 7.5 fs is used for the light source. The absorption of the structure is measured at different frequencies.

3. Results and Discussion

In this section, the adopted MMA structure depicted in Figure 1 is optimized to maximize the absorption of the device over a broad spectral band from 100 to 1000 GHz. First, the absorption of the MMA is measured using Lumerical FDTD solution software for different rod materials, then the dielectric substrate material is optimized, and finally, the geometric dimensions of the rod are optimized.

3.1. Effect of the Rod Material on the Absorption of the MMA

The MMA is simulated for different nanorod materials to elect the material that maximizes the absorption. Figure 2 shows the absorption of the MMA, with SiO_2 dielectric substrate, measured when all nanorods are made from gold, and Aluminum. Furthermore, the absorption is measured when the nanorods are arranged such that aluminum and gold rows are alternating as shown in Figure 3. The height and radius of the nanorods are h = 50 nm and radius r = 60 nm, respectively, and the height of the dielectric substrate is chosen as h_1 = 60 nm. It is clear from Figure 2 that the absorber with Au nanorods has better absorption than the absorber with Al nanorods in high frequency range from 600 to 1000 GHz, while the opposite behavior is observed in the lower frequency range from 300 to 600 GHz. Using alternating rows of Au, and Al, the absorption is somewhere between that of the two cases.

The absorption of the MMA depends on the material of the nanorods as the resonance frequency depends on the current generated in the metallic nanorods and the generated plasmons which depend on the material. Additionally, according to the RLC model of the MMA, absorption depends on the losses in the dielectric material and ohmic losses of the nanorods [40]. The average absorptions in the three cases are calculated by finding the area under each curve divided by the frequency span (1000–100 GHz). The obtained average absorption values are 72.09%, 69.94%, and 73.56% in case of Au nanorods, Al nanorods, and alternating rows of Au and Al nanorods, respectively. Hence, the design of the typical structure is modified to that shown in Figure 3 with alternating rows of Au, and Al nanorods.

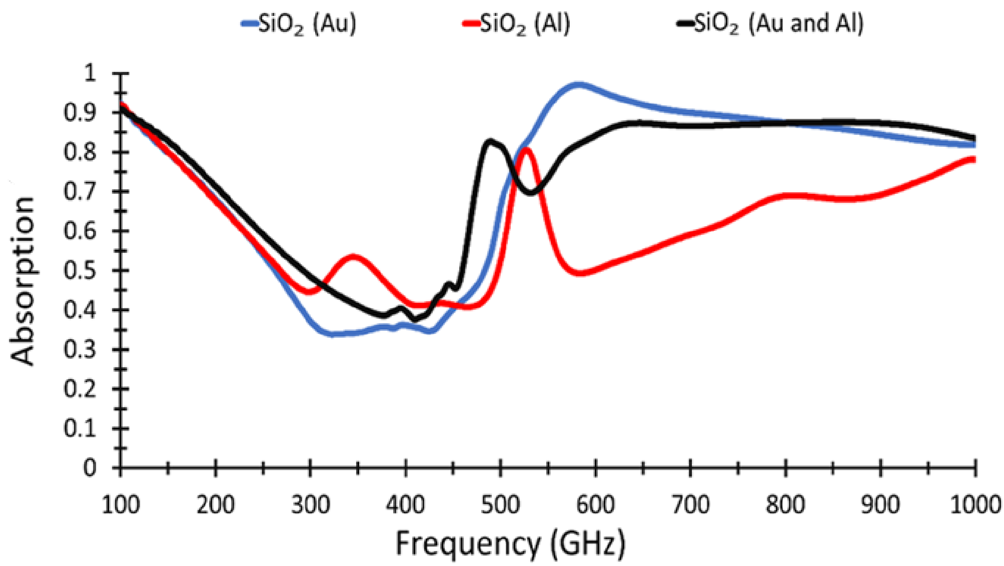

Figure 2. Absorption of the MMA structure.

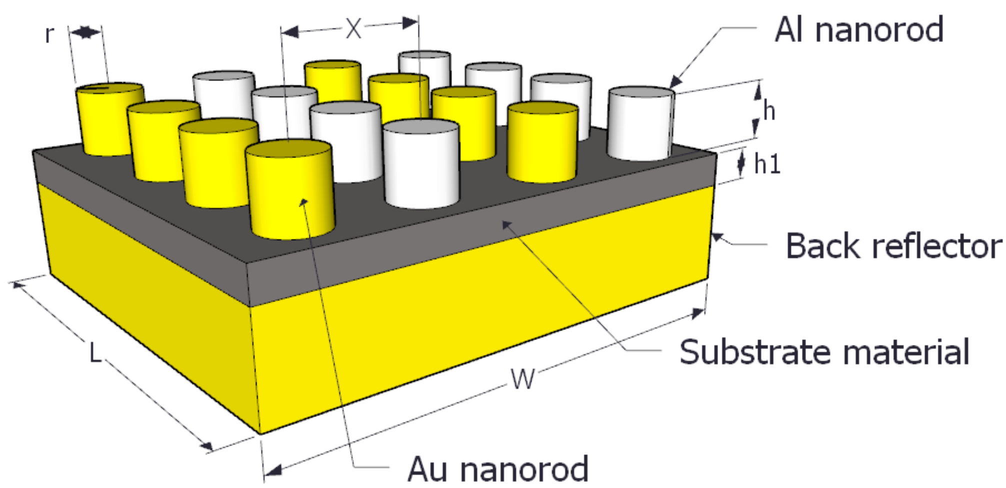

Figure 3. Schematic diagram of the MMA structure with alternating rows of Au, and Al.

3.2. Effect of the Dielectric Substrate Material on the Absorption of the MMA

The absorption of the modified MMA structure shown in Figure 3 is investigated with different dielectric substrate materials of 60 nm fixed thickness. The dimensions of each nanorod in the alternating rows of Au, Al are fixed to h = 50 nm and radius r = 60 nm. Figure 4 shows the absorption of the MMA structure, with Al_2O_3, SiO_2, and TiO_2 substrates. The absorption of the MMA with SiO_2 substrate is the highest in the longer frequency ranging from 600 to 1000 GHz, while the MMA absorber with TiO_2 substrate has the worst absorption over this frequency range. The maximum absorption using SiO_2 substrate exceeds 95%, but the MMA with TiO_2 substrate has the best absorption over the frequency range below 450 GHz with 96% absorption peak at 363 GHz, and another 92% peak at 423 GHz. According to Equation (6), the absorption of the MMA depends on the input impedance of the absorber, which depends on the permittivity, permeability, and refractive index of the dielectric substrate [21].

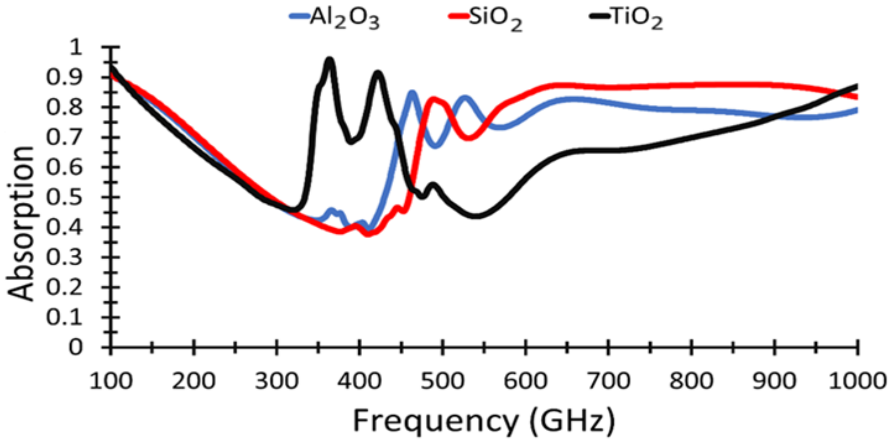

Figure 4. Absorption of the modified structure using different dielectric substrate materials.

The average power absorbed by the MMA is calculated from the obtained absorption spectrum and the absorbed power is 73.6%, 71%, and 70% for SiO_2, Al_2O_3, and TiO_2 dielectric substrates, respectively.

As MMAs with SiO_2, or Al_2O_3, give a high absorption in the frequency range above 600 GHz, and MMA with TiO_2 substrate has its peak absorption in the frequency range below 450 GHz, in the next stage, the absorption of the absorber is investigated with multi-dielectric layers substrate, as shown in Figure 5.

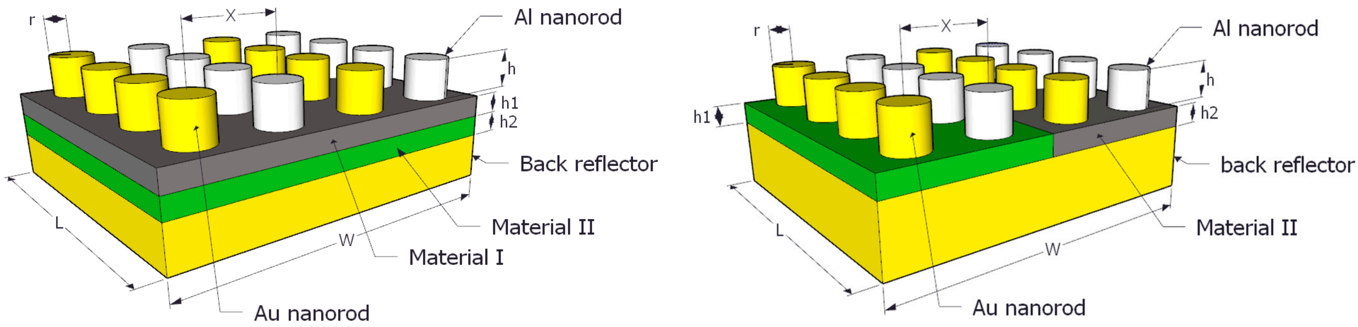

(**a**) (**b**)

Figure 5. Modified MMA substrate with multi-dielectric layers substrate: (**a**) Two substrates on top of each other; (**b**) two side-by-side substrates.

The performance of the absorber is investigated in two cases. The first case is shown in Figure 5a, where the two substrates are on top of each other, while in the second case shown in Figure 5b, the dielectric substrates are side-by-side, each sharing 50% of the ground plate area. All combinations of SiO_2, Al_2O_3, and TiO_2 dielectric substrates are tested to elect the substrate that will give better absorption over a wider band. The absorption of the MMA for the first case is shown in Figure 6a, and for second case is shown in Figure 6b. The difference in the absorption of the absorber between case 1 and case 2 is because of the different overall equivalent capacitance of the absorber which in turn changes the input impedance of the absorber and affects its absorption. The minimum absorption, maximum absorption and average absorption are listed in Table 2.

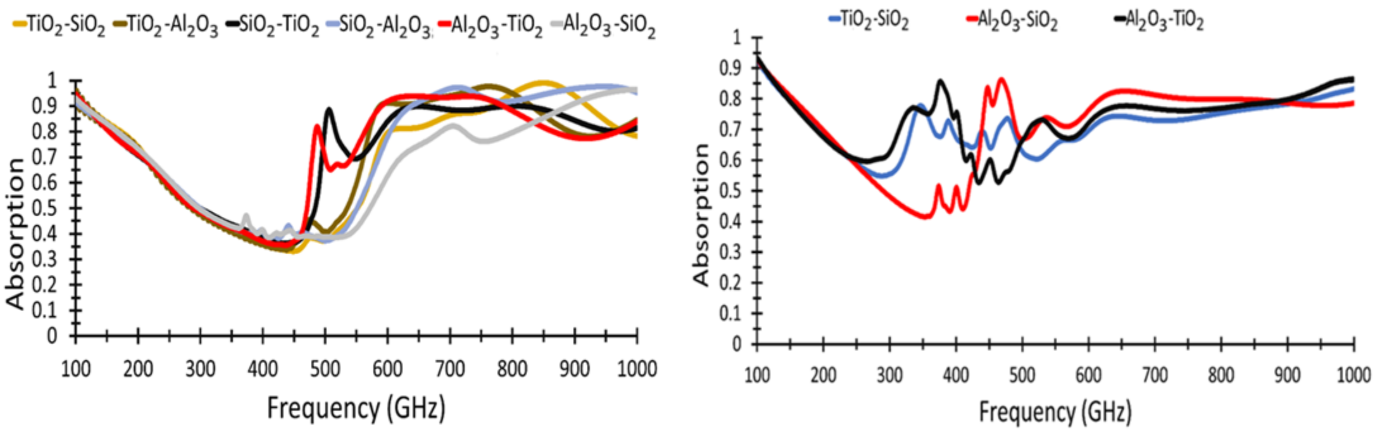

(**a**) (**b**)

Figure 6. Absorption of the multi-dielectric layers MMA structure: (**a**) Two dielectric layers on top of each other; (**b**) Two side-by-side dielectric layers.

Table 2. Absorption for different dielectric substrates.

	Dielectric Substrate Material	Minimum Absorption	Maximum Absorption	Average Absorption
Single dielectric layer	SiO_2	37.6%	90.8%	73.6%
	Al_2O_3	39.4%	91.4%	71.0%
	TiO_2	43.7%	96.1%	70.0%
Multi-dielectric layers on top of each other (The first one is the upper layer)	TiO_2-SiO_2	33.2%	99.0%	69.8%
	TiO_2-Al_2O_3	33.7%	97.7%	71.0%
	SiO_2-TiO_2	36.3%	93.5%	72.4%
	SiO_2-Al_2O_3	37.3%	97.7%	72.7%
	Al_2O_3-TiO_2	35.6%	94.7%	72.7%
	Al_2O_3-SiO_2	38.5%	96.4%	67.4%
Side-by-side multi-dielectric layers	TiO_2-SiO_2	54.8%	92.7%	71.6%
	Al_2O_3-SiO_2	41.5%	92.7%	71.5%
	TiO_2-Al_2O_3	52.6%	93.3%	73.4%

The calculated data presented in Table 1 shows that the absorption of the device is affected by the position of the dielectric layer, and the highest absorption is achieved when the multi-dielectric layers are TiO_2-SiO_2 with SiO_2 is the bottom layer. It's reported that when the top layer is a strong absorber, then the overall absorption of the whole device increases. Small reflection coefficient (S_{11}) of the top layer is a crucial requirement [41]. Furthermore, the minimum absorption is enhanced from 37.6%, and 43.7% in case of single SiO_2, and single TiO_2 layer, respectively, to 54.8% when side-by-side TiO_2-SiO_2 layers are used. This means that the minimum absorption increases by a factor between 25.4% and 46%. Hence, the TiO_2-SiO_2 side-by-side multi-dielectric layers structure with 71.6% average absorption is elected for further enhancement.

3.3. Effect of the Au, Al Array Distribution and Rod Dimensions on the Absorption of the MMA

The structure is modified for further investigation, the nanorod distribution is changed from the alternating rows of nanorods shown in Figure 5b to alternating Au, Al nanorods, so each nanorod is surrounded by four nanorods of the other material as shown in Figure 7.

The absorption of the structure is shown in Figure 8. As an effect of the new nanorods distribution, average power absorption is elevated to 75.7%, the maximum absorption is increased to 94.2%, while the minimum absorption becomes 59.3%.

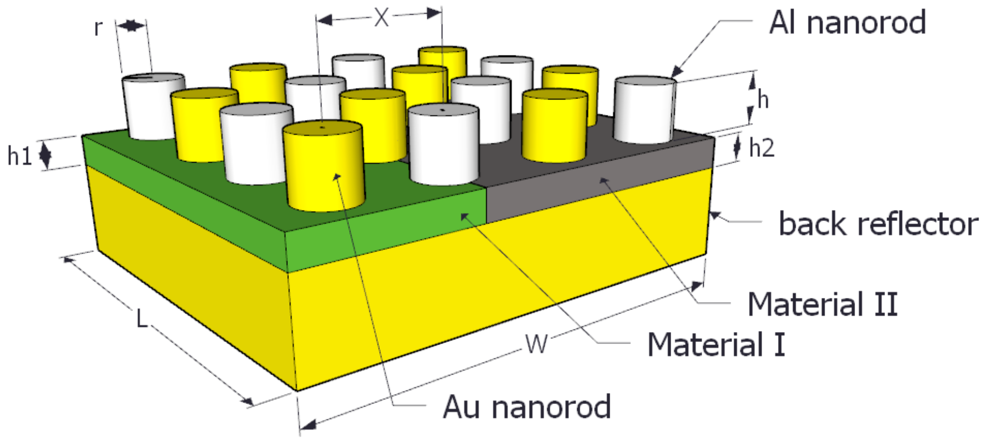

Figure 7. MMA side-by-side multi-dielectric layers structure with alternating nanorods distribution.

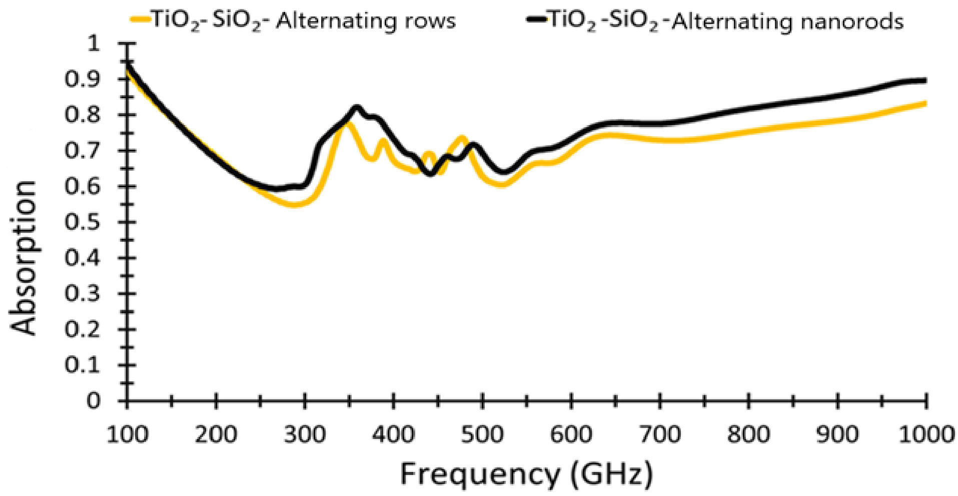

Figure 8. Absorption of the side-by-side multi-dielectric layers MMA structure with alternating rows of nanorods and alternating nanorods.

The distribution of the nanorods changes the distribution of the local surface plasmons induced which affects the electric field in the dielectric material. The absorption of the electromagnetic wave in the dielectric material depends on the magnitude squared ($|E|^2$) of the electric field, which is strongly affected by the design of the structure.

The effect of the radius of the nanorods on the absorption of the MMA is investigated. The radius of the alternating Au, Al nanorods is changed from 40 to 70 nm, while the rod height is fixed to 50 nm, and the absorption is measured in each case. The obtained results are shown in Figure 9a. The effect of the radius is neglected as the maximum absorption is about 94% for all cases and the minimum absorption is between 59.3% and 60%. Moreover, there is a small variation in average absorbed power between 76% and 77%. In addition, the nanorod height is changed from 50 to 80 nm to be optimized. The absorption decreased to almost zero around 400 GHz with nanorods of height 70 nm and 80 nm and increased at the same frequency to 95% with nanorods of height 50 nm then decreased to 55% at 300 GHz, as illustrated in Figure 9b. The optimum nanorod radius and height are 50 nm and 60 nm, respectively.

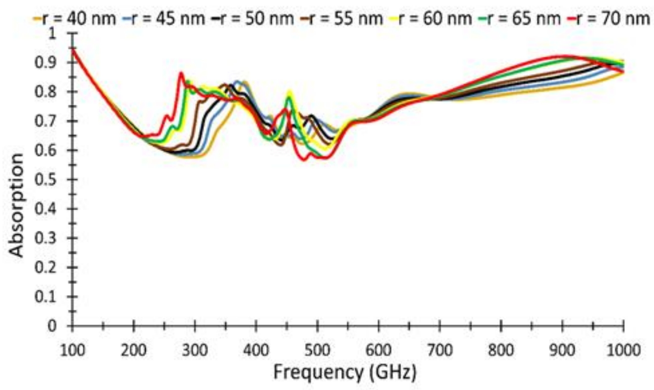

(a)

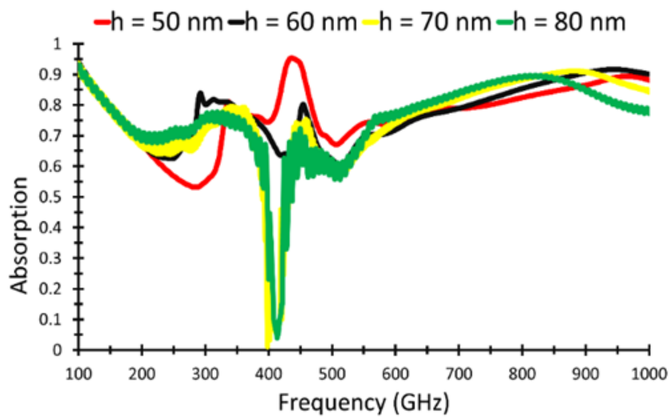

(b)

Figure 9. Absorption of the side-by-side multi-dielectric layers MMA structure with alternating nanorods with: (**a**) varying radius from 40 to 70 nm; (**b**) varying heights from 50 to 80 nm.

Finally, a ZnO layer of different thicknesses, 40–70nm, is added on top of the Au ground plate. Recently, ZnO is used to increase the interaction of incident electromagnetic waves and the substrate dielectric layer and thus increase the absorption of the MMA over the operating frequency range [42]. The measured absorption without the ZnO layer and with the ZnO layer of different thicknesses is shown in Figure 10. Adding ZnO layer slightly increases the maximum absorption as illustrated in Table 3. According to the following optimization steps, the optimized structure is shown in Figure 11, where a ZnO layer of thickness 60 nm is added on top of the back reflector. Hence, the optimum design gives an average absorption of 84%, minimum absorption of 65.9% and maximum absorption of 100%.

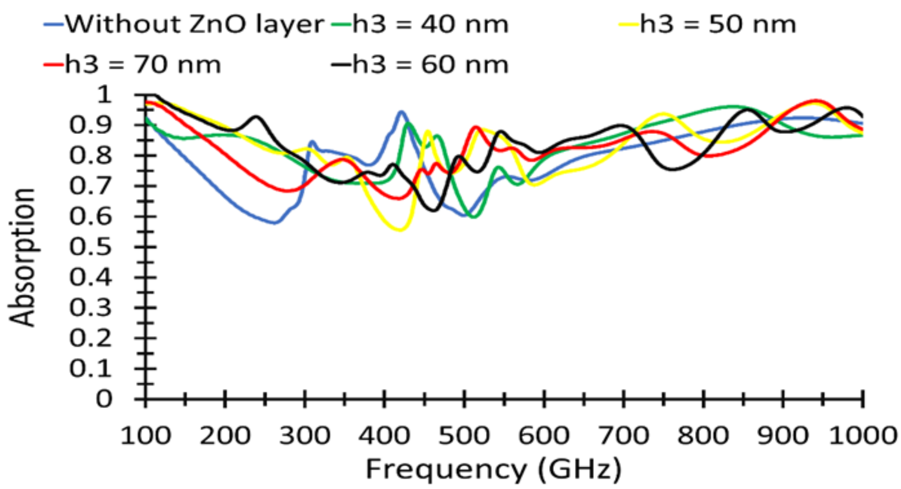

Figure 10. Effect of adding ZnO layer with different thicknesses, 40–70 nm, on the absorption of the absorber.

The enhanced absorption is illustrated in Figure 12 when the ZnO layer is grown on top of the Au layer and used as a base for TiO_2-SiO_2 materials. The absorption is more than 80% in three different regions, 100–280 GHz, 530–740 GHz and 800–1000 GHz, which represent almost 95% of the band. On the other hand, the obtained absorption is more than 65% in the range from 100 GHz to 1000 GHz.

Table 3. Absorption for different dielectric substrates.

ZnO Layer Thickness	Minimum Absorption	Maximum Absorption	Average Absorption
Without ZnO layer	59.3%	94.0%	77.0%
h_3 = 40 nm	60.0%	95.7%	83.3%
h_3 = 50 nm	55.5%	94.9%	83.5%
h_3 = 60 nm	65.9%	100%	84.0%
h_3 = 70 nm	62.4%	95.1%	82.1%

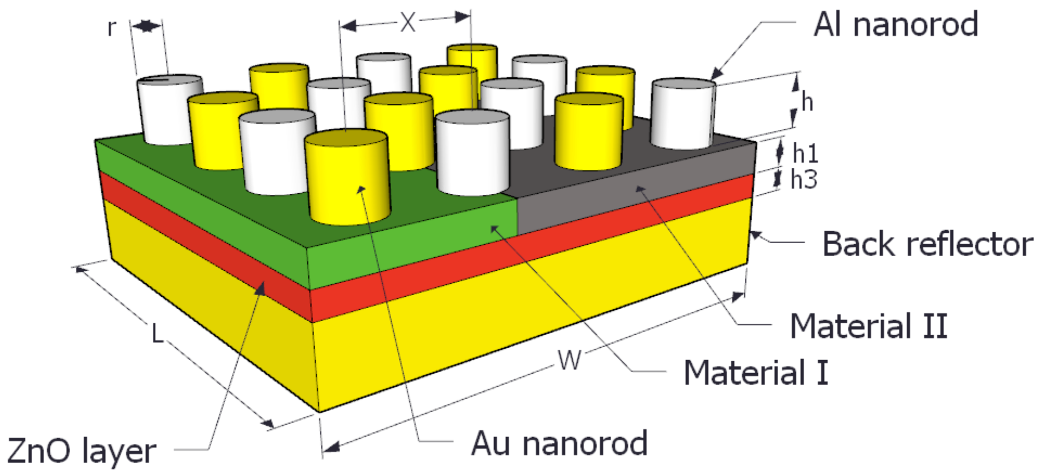

Figure 11. MMA side-by-side multi-dielectric layers structure with alternating nanorods distributed on ZnO substrate.

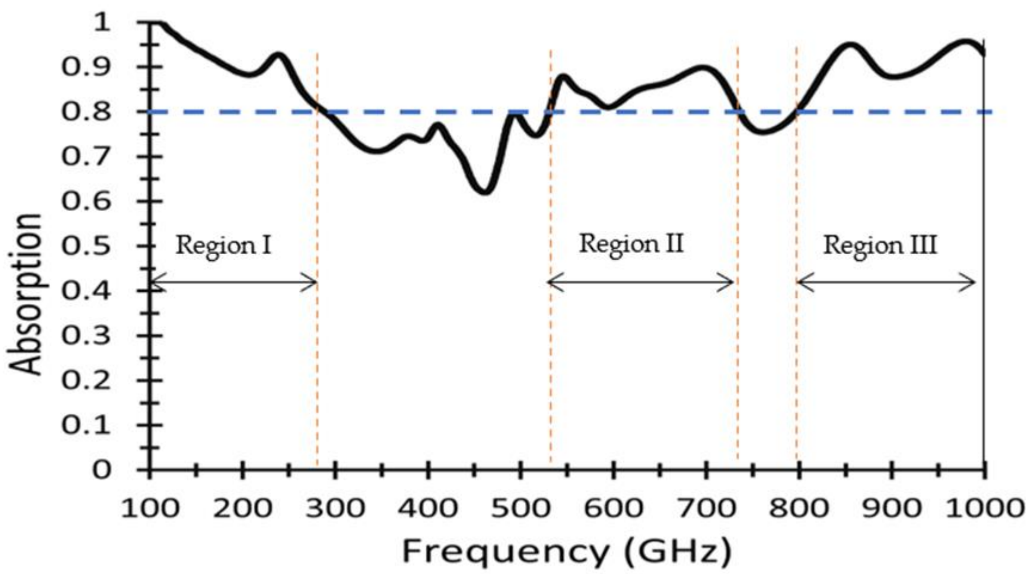

Figure 12. The optimum absorption is more than 65% in the range 100–1000 GHz, and with 65.5% of the band over 80% absorption.

The electric field and magnetic field distributions and absorbed optical power are shown in Figure 13 at three different frequencies (230, 450, and 700 GHz). At 450 GHz, there is an electric and magnetic resonance in the TiO_2 layer where the maximum power is absorbed. On the other hand, at 700 GHz, the electric and magnetic field resonance occurs in the SiO_2 and the ZnO layer where the maximum power absorption takes place. Moreover, some power is absorbed by the plasmonic nanorods. The effect the ZnO layer is clear at 700 GHz, as the absorbed power increased due the power absorbed in the ZnO layer. At

450 GHz, where one minimum absorption occurs, Figure 13 shows that no resonance occurs at this frequency which leads to minimum power absorption shown at this frequency.

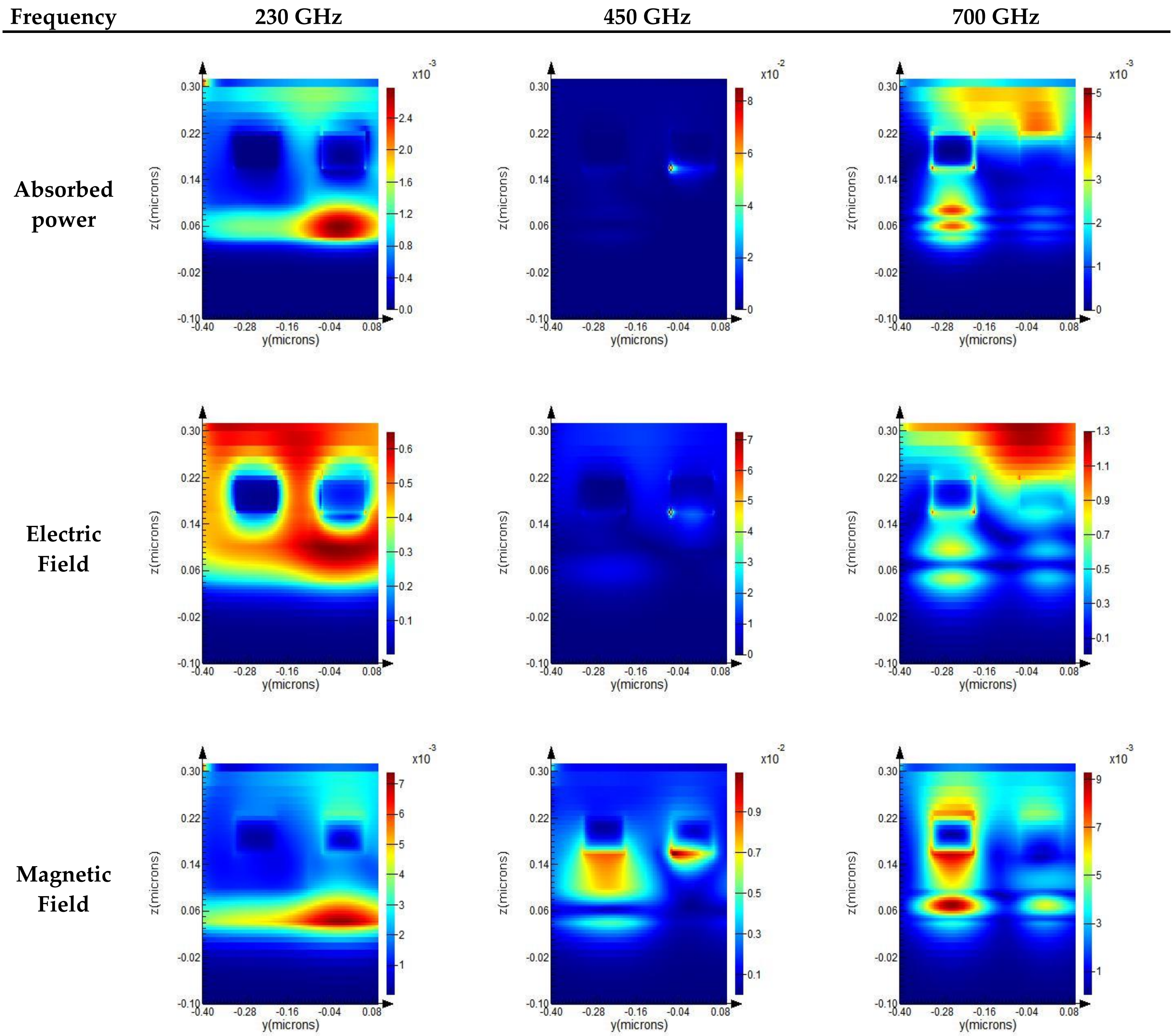

Figure 13. Absorbed optical power, electric field distribution, and magnetic field distribution in the proposed MMA structure at different frequencies.

3.4. *Effect of the Incidence Angle and Light Polarization on the Absorption of the MMA*

The direction of the incident light and its polarization play an important role in the performance the MMA, so this effect is investigated in this section. Figure 14 shows the absorption of the MMA for different incident angles ranging from 0° (normal incidence) to 70° in a step of 10°. Changing the incidence angle, slightly alters the performance of the absorber with some ripples are observed in the absorbed power. The minimum, maximum, and average power absorbed at different angles are shown in Table 4. The maximum absorbed power changes over a range from 100% to 98.6% which represents a 1.4% decrease in maximum absorption. While the average absorption changes from 84% to 93.3% (about 11% increase), the minimum absorption increases from 65.9% to 78.4% at 50°. Practically, the incident wave is far away from the object and angular stability over a 30° range is enough to ensure absorber stability [20].

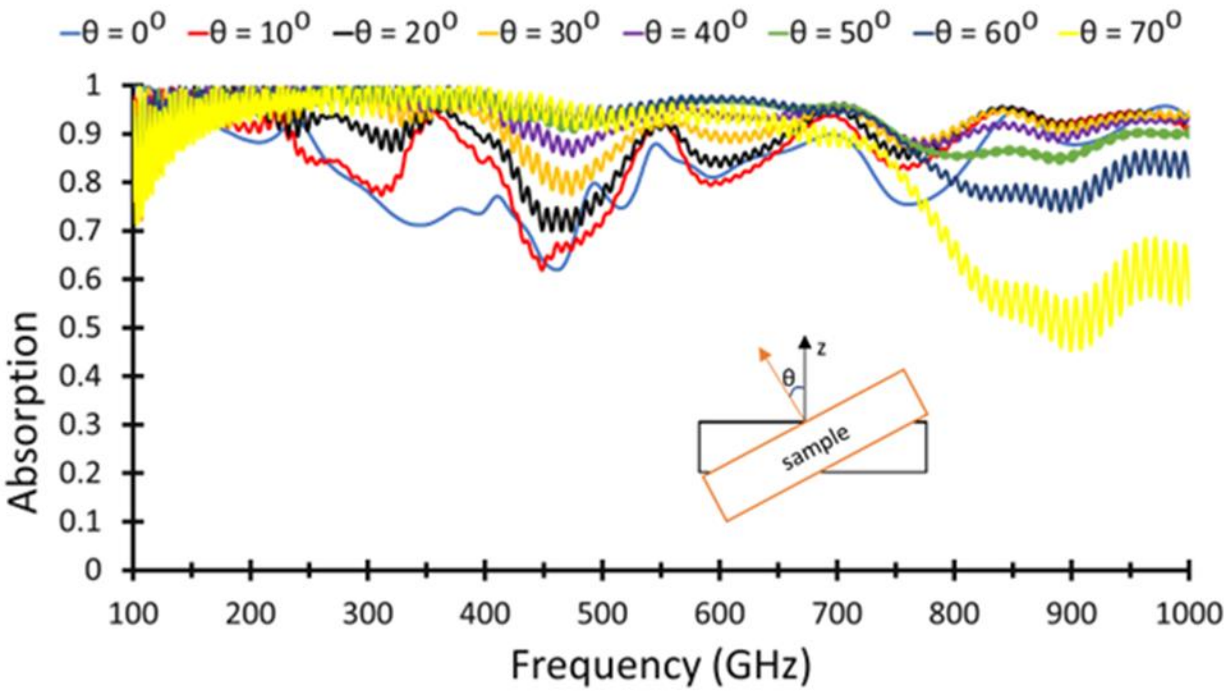

Figure 14. Absorption of the proposed optimized MMA structure for different incident angles.

Table 4. Absorption for different values of incident angle.

θ = 0°	Minimum Absorption	Maximum Absorption	Average Absorption
Direct	65.9%	100%	84%
10°	61.8%	99.1%	86.9%
20°	70.3%	98.8%	89.9%
30°	72.1%	98.6%	92.1%
40°	77.5%	98.8%	93.3%
50°	78.4%	99.1%	93.3%
60°	63.4%	99.1%	91.5%
70°	45%	98.8%	84.5%

The effect of light polarization is investigated by changing the direction of light polarization angle from 0° to 90° in a step of 15°, as shown in Figure 15. Due to the symmetry of the proposed structure, light polarization has no effect on the absorbed power. The effect of light polarization is then investigated for oblique incidence case where the incident angle is 30° and the obtained absorption is shown in Figure 16. It is clear from Figure 16 that the proposed structure is insensitive to light polarization in oblique incidence as well.

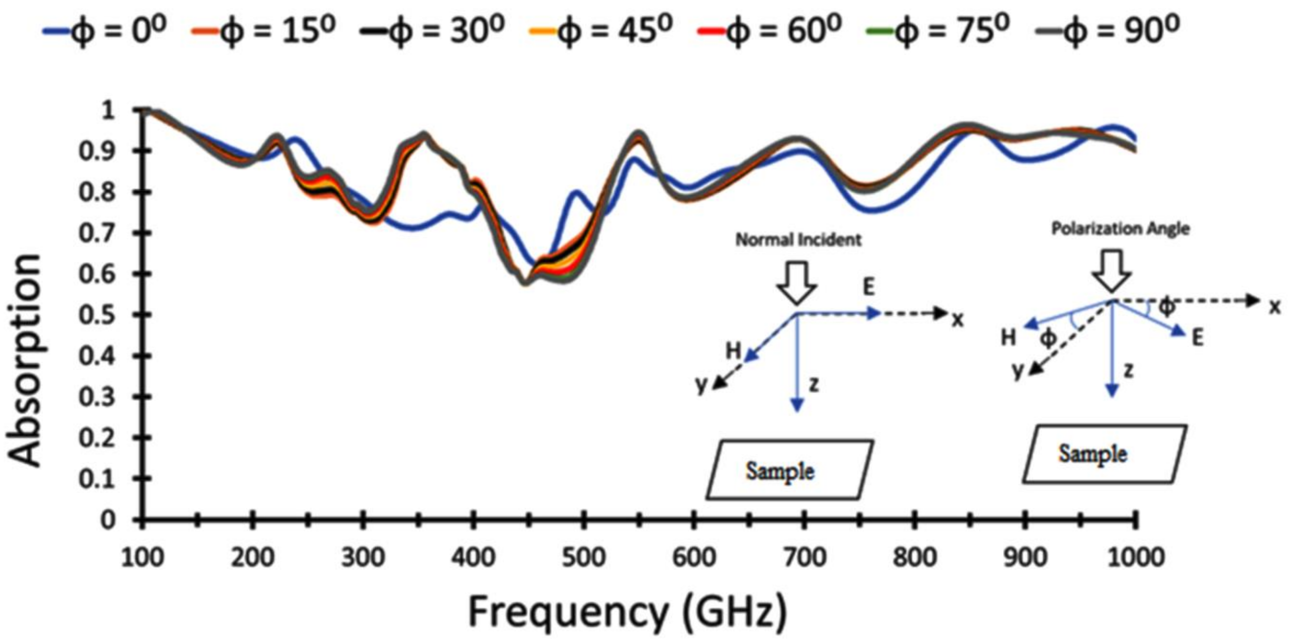

Figure 15. Absorption of the proposed optimized MMA structure for different light polarization at normal incidence.

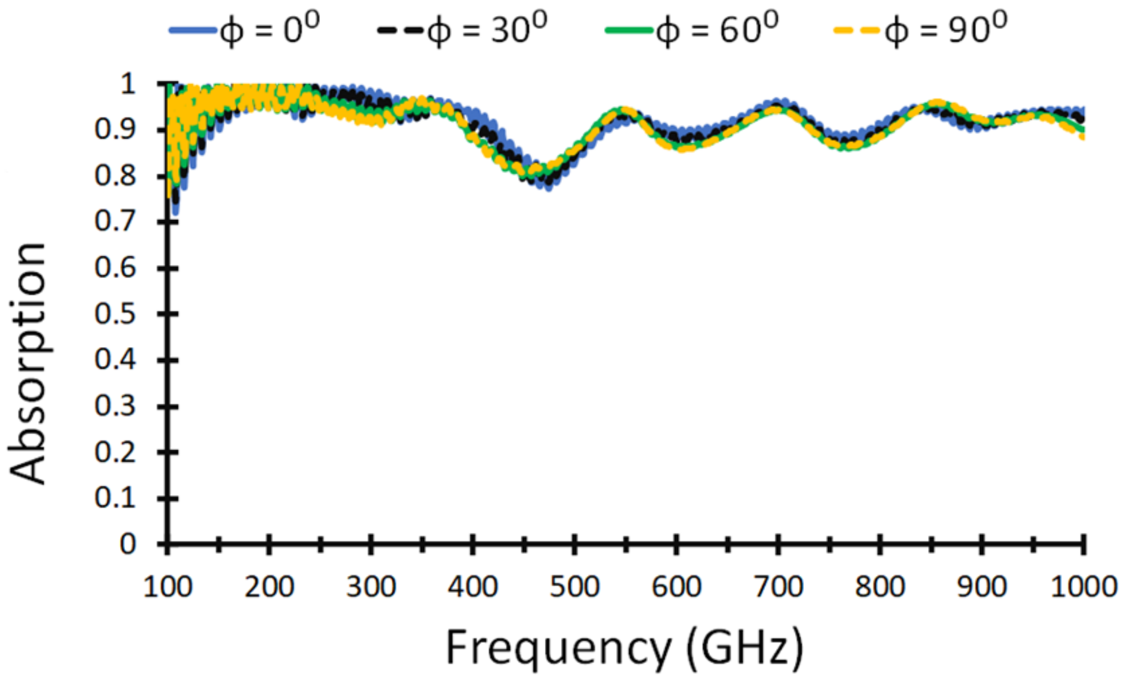

Figure 16. Absorption of the proposed optimized MMA structure for different light polarization at oblique incidence (θ = 30°).

The development of a broadband MMA operating in the wide range of the spectrum has been challenging until now, but comparing our results with the recently reported MMAs shows that the proposed MMA in this work has larger broadband, from 100 to 1000 GHz, with high maximum absorption 100%. The comparison of the absorber's performance is listed in Table 5.

Table 5. Comparison of the MMA performance with recently reported MMAs.

Related Work	Operating Frequency Range	Maximum Absorption	Technique
Ref. [43]	25–37.5 THz	87%	Ti/Ge/Si_3N_4/Ti metamaterial structure
Ref. [44]	6–16 GHZ	Exceeds 80%	Metallic strips fabricated with lumped resistors on a FR-4 substrate
Ref. [45]	0.79–20.9 GHz and 25.1–40 GHz	90%	Magnetic absorbing material and a multi-layered meta-structure
Ref. [46]	4.2–7.4 THz	98.21%	Split gold and graphene rings over a dielectric and gold plate.
Ref. [47]	7.22–8.84 GHz	90%	Asymmetric section resonator structure with different sizes.
Ref. [48]	10–17 GHz	90%	Array of alternating copper, and FR-4 disks to form a conical frustum
Proposed structure	100–1000 GHz	100%	Au nanorods/TiO_2-SiO_2/Au ground plate metamaterial structure

4. Conclusions

In this work, a metamaterial absorber structure with multi-dielectric layer is introduced. The structure is optimized to maximize the absorption of the MMA and enhance the minimum absorption of it using SiO_2-TiO_2 side-by-side multi-dielectric layer on top of a ground Au plate, and an alternating Au, Al nanorods on the dielectric substrate. The ZnO layer is added as a substrate on the top of Au back reflector to enhance the absorption. The MMA has an average absorption of 84%%, a maximum absorption of 100%, and a minimum absorption of about 65.9%. The optimized MMA is shown to have good angular stability as the effect of the incident angle of the electromagnetic wave on the MMA absorption is so small and the absorber is insensitive to polarization for both normal and oblique incidence conditions.

Author Contributions: Methodology, B.E., A.E. (Ahmed Emara) and A.Y.; software, A.E. (Ali Elrashidi) and G.J.; validation, B.E., A.Y. and G.J.; formal analysis, A.E. (Ali Elrashidi) and A.E. (Ahmed Emara); investigation, B.E. and G.J.; resources, A.E. (Ahmed Emara); writing—original draft preparation, A.E. (Ali Elrashidi) and A.Y.; writing—review and editing, G.J.; supervision, A.E. (Ahmed Emara) and G.J. All authors have read and agreed to the published version of the manuscript.

Funding: This research received no external funding.

Data Availability Statement: Not applicable.

Conflicts of Interest: The authors declare no conflict of interest.

Appendix A

The real part and imaginary part of the dielectric constant of the used materials are in the material database of the Lumerical software. These dielectric constant values are shown in Figures A1–A4 for Al_2O_3, SiO_2, TiO_2, and ZnO, respectively.

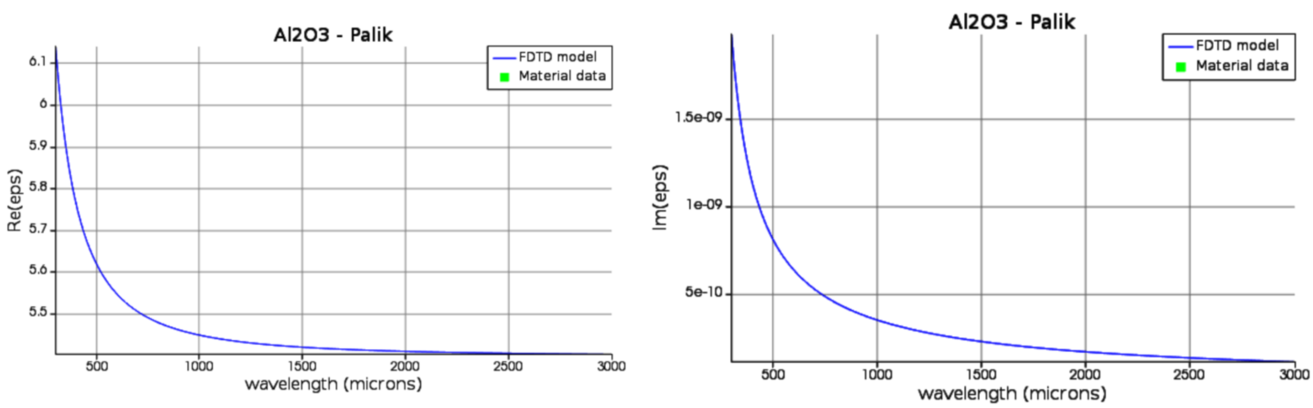

(**a**) (**b**)

Figure A1. Dielectric constant of Al_2O_3: (**a**) The real part of the dielectric constant; (**b**) The imaginary part of the dielectric constant.

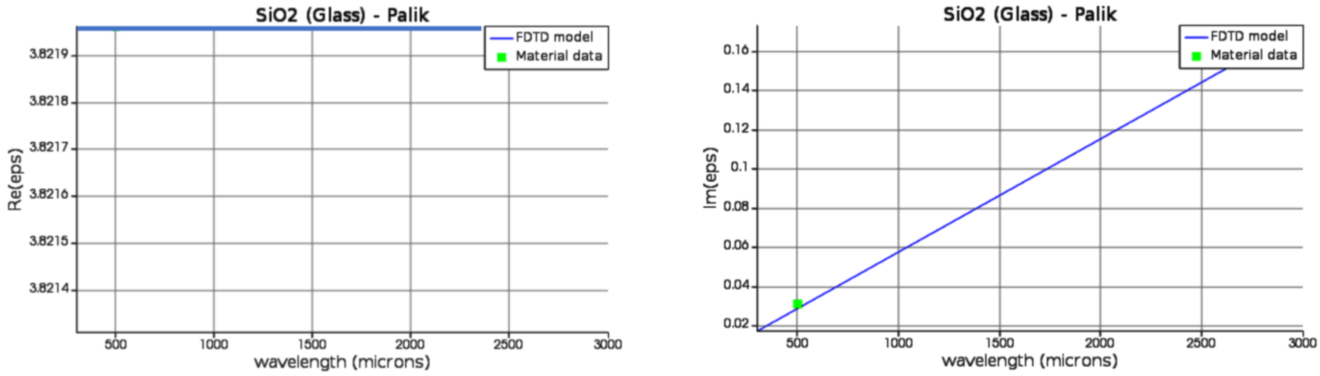

(**a**) (**b**)

Figure A2. Dielectric constant of SiO_2: (**a**) The real part of the dielectric constant; (**b**) The imaginary part of the dielectric constant.

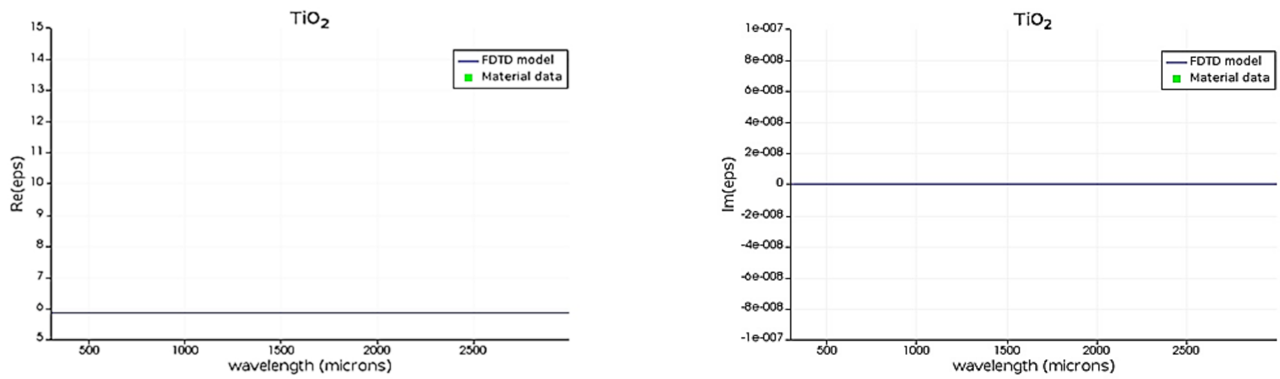

(**a**) (**b**)

Figure A3. Dielectric constant of TiO_2: (**a**) The real part of the dielectric constant; (**b**) The imaginary part of the dielectric constant.

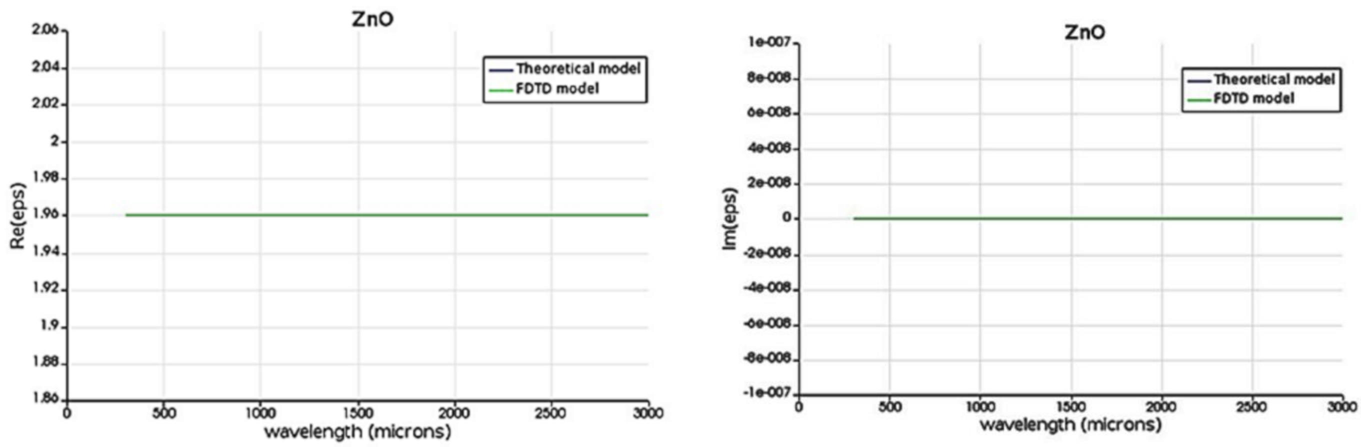

(**a**) (**b**)

Figure A4. Dielectric constant of ZnO: (**a**) The real part of the dielectric constant; (**b**) The imaginary part of the dielectric constant.

References

1. Monti, A.; Toscano, A.; Bilotti, F. Exploiting the Surface Dispersion of Nanoparticles to Design Optical-Resistive Sheets and Salisbury Absorbers. *Opt. Lett.* **2016**, *41*, 3383–3386. [CrossRef] [PubMed]

2. Medvedev, V.V.; Novikova, N.N.; Zoethout, E. Salisbury Screen with Lossy Nonconducting Materials: Way to Increase Spectral Selectivity of Absorption. *Thin Solid Film.* **2022**, *751*, 139232. [CrossRef]
3. Wulan, Q.; He, D.; Zhang, T.; Peng, H.; Liu, L.; Medvedev, V.V.; Liu, Z. Salisbury Screen Absorbers Using Epsilon-near-Zero Substrate. *Mater. Res. Express* **2021**, *8*, 16406. [CrossRef]
4. Fang, X.; Zhao, C.Y.; Bao, H. Design and Analysis of Salisbury Screens and Jaumann Absorbers for Solar Radiation Absorption. *Front. Energy* **2018**, *12*, 158–168. [CrossRef]
5. Oh, J.; Choi, J. *Adaptable Compressed Jaumann Absorber for Harsh and Dynamic Electromagnetic Environments*; Syracuse Univ Ny Syracuse: Syracuse, NY, USA, 2020.
6. Ma, Z.; Jiang, C.; Cao, W.; Li, J.; Huang, X. An Ultrawideband and High-Absorption Circuit-Analog Absorber with Incident Angle-Insensitive Performance. *IEEE Trans. Antennas Propag.* **2022**. [CrossRef]
7. Yao, Z.; Xiao, S.; Li, Y.; Wang, B. Wide-Angle, Ultra-Wideband, Polarization-Independent Circuit Analog Absorbers. *IEEE Trans. Antennas Propag.* **2022**, *70*, 7276–7281. [CrossRef]
8. Landy, N.I.; Sajuyigbe, S.; Mock, J.J.; Smith, D.R.; Padilla, W.J. Perfect Metamaterial Absorber. *Phys. Rev. Lett.* **2008**, *100*, 207402. [CrossRef]
9. Bagmanci, M.; Karaaslan, M.; Unal, E.; Akgol, O.; Bakır, M.; Sabah, C. Solar Energy Harvesting with Ultra-Broadband Metamaterial Absorber. *Int. J. Mod. Phys. B* **2019**, *33*, 1950056. [CrossRef]
10. Shuvo, M.M.K.; Hossain, M.I.; Mahmud, S.; Rahman, S.; Topu, M.T.H.; Hoque, A.; Islam, S.S.; Soliman, M.S.; Almalki, S.H.A.; Islam, M. Polarization and Angular Insensitive Bendable Metamaterial Absorber for UV to NIR Range. *Sci. Rep.* **2022**, *12*, 1–15. [CrossRef]
11. Wu, J.; Sun, Y.; Wu, B.; Sun, C.; Wu, X. Perfect Metamaterial Absorber for Solar Energy Utilization. *Int. J. Therm. Sci.* **2022**, *179*, 107638. [CrossRef]
12. Hossain, M.J.; Faruque, M.R.I.; Islam, M.T. Perfect Metamaterial Absorber with High Fractional Bandwidth for Solar Energy Harvesting. *PLoS ONE* **2018**, *13*, e0207314. [CrossRef] [PubMed]
13. Abdulkarim, Y.I.; Deng, L.; Altıntaş, O.; Ünal, E.; Karaaslan, M. Metamaterial Absorber Sensor Design by Incorporating Swastika Shaped Resonator to Determination of the Liquid Chemicals Depending on Electrical Characteristics. *Phys. E Low-Dimens. Syst. Nanostruct.* **2019**, *114*, 113593. [CrossRef]
14. Gao, Z.; Fan, Q.; Tian, X.; Xu, C.; Meng, Z.; Huang, S.; Xiao, T.; Tian, C. An Optically Transparent Broadband Metamaterial Absorber for Radar-Infrared Bi-Stealth. *Opt. Mater.* **2021**, *112*, 110793. [CrossRef]
15. Chen, X.; Tian, C.; Che, Z.; Chen, T. Selective Metamaterial Perfect Absorber for Infrared and 1.54 Mm Laser Compatible Stealth Technology. *Optik* **2018**, *172*, 840–846. [CrossRef]
16. Naveed, M.A.; Bilal, R.M.H.; Baqir, M.A.; Bashir, M.M.; Ali, M.M.; Rahim, A.A. Ultrawideband Fractal Metamaterial Absorber Made of Nickel Operating in the UV to IR Spectrum. *Opt. Express* **2021**, *29*, 42911–42923. [CrossRef]
17. Telha, S.; Nouho, A.A.; Ibrahim, I.A.; Achaoui, Y.; Bouaaddi, A.; Jakjoud, H.; Baida, F.I. Annular Hole Array Design as a High Efficiency Absorber for Photovoltaic Applications. *Optik* **2022**, *268*, 169735. [CrossRef]
18. Cheng, Y.; Zou, Y.; Luo, H.; Chen, F.; Mao, X. Compact Ultra-Thin Seven-Band Microwave Metamaterial Absorber Based on a Single Resonator Structure. *J. Electron. Mater.* **2019**, *48*, 3939–3946. [CrossRef]
19. Zhou, Q.; Yin, X.; Ye, F.; Mo, R.; Tang, Z.; Fan, X.; Cheng, L.; Zhang, L. Optically Transparent and Flexible Broadband Microwave Metamaterial Absorber with Sandwich Structure. *Appl. Phys. A* **2019**, *125*, 1–8. [CrossRef]
20. Lai, S.; Wu, Y.; Zhu, X.; Gu, W.; Wu, W. An Optically Transparent Ultrabroadband Microwave Absorber. *IEEE Photonics J.* **2017**, *9*, 1–10. [CrossRef]
21. Ning, J.; Chen, K.; Zhao, W.; Zhao, J.; Jiang, T.; Feng, Y. An Ultrathin Tunable Metamaterial Absorber for Lower Microwave Band Based on Magnetic Nanomaterial. *Nanomaterials* **2022**, *12*, 2135. [CrossRef]
22. Hossain, M.B.; Faruque, M.R.I.; Islam, M.T.; Singh, M.; Jusoh, M. Triple Band Microwave Metamaterial Absorber Based on Double E-Shaped Symmetric Split Ring Resonators for EMI Shielding and Stealth Applications. *J. Mater. Res. Technol.* **2022**, *18*, 1653–1668. [CrossRef]
23. Guo, W.; Liu, Y.; Han, T. Ultra-Broadband Infrared Metasurface Absorber. *Opt. Express* **2016**, *24*, 20586–20592. [CrossRef] [PubMed]
24. Kang, Y.; Gao, P.; Liu, H.; Gao, L. A Polarization-Insensitive Dual-Band Plasmonic Metamaterial Absorber for a Sensor Application. *Phys. Scr.* **2021**, *96*, 65804. [CrossRef]
25. Katrodiya, D.; Jani, C.; Sorathiya, V.; Patel, S.K. Metasurface Based Broadband Solar Absorber. *Opt. Mater.* **2019**, *89*, 34–41. [CrossRef]
26. Xu, W.Z.; Ye, Z.Z.; Zeng, Y.J.; Zhu, L.P.; Zhao, B.H.; Jiang, L.; Lu, J.G.; He, H.P.; Zhang, S.B. ZnO light-emitting diode grown by plasma-assisted metal organic chemical vapor deposition. *Appl. Phys. Lett.* **2006**, *88*, 173506. [CrossRef]
27. Chu, S.; Olmedo, M.; Yang, Z.; Kong, J.; Liu, J. Electrically pumped ultraviolet ZnO diode lasers on Si. *Appl. Phys. Lett.* **2008**, *93*, 181106. [CrossRef]
28. Robertson, J. High dielectric constant oxides. *Eur. Phys. J.-Appl. Phys.* **2004**, *28*, 265–291. [CrossRef]
29. Dette, C.; Pérez-Osorio, M.A.; Kley, C.S.; Punke, P.; Patrick, C.E.; Jacobson, P.; Giustino, F.; Jung, S.J.; Kern, K. TiO_2 anatase with a bandgap in the visible region. *Nano Lett.* **2014**, *14*, 6533–6538. [CrossRef]

30. Li, Z.; Rusli, E.; Foldyna, M.; Wang, J.; Chen, W.; Prakoso, A.B.; Lu, C.; i Cabarrocas, P.R. Nanostructured Back Reflectors Produced Using Polystyrene Assisted Lithography for Enhanced Light Trapping in Silicon Thin Film Solar Cells. *Sol. Energy* **2018**, *167*, 108–115. [CrossRef]
31. Hsu, C.; Burkhard, G.F.; McGehee, M.D.; Cui, Y. Effects of Nanostructured Back Reflectors on the External Quantum Efficiency in Thin Film Solar Cells. *Nano Res.* **2011**, *4*, 153–158. [CrossRef]
32. Li, H.; Yuan, L.H.; Zhou, B.; Shen, X.P.; Cheng, Q.; Cui, T.J. Ultrathin Multiband Gigahertz Metamaterial Absorbers. *J. Appl. Phys.* **2011**, *110*, 14909. [CrossRef]
33. Ogawa, S.; Kimata, M. Metal-Insulator-Metal-Based Plasmonic Metamaterial Absorbers at Visible and Infrared Wavelengths: A Review. *Materials* **2018**, *11*, 458. [CrossRef] [PubMed]
34. Zhang, M.; Song, Z. Switchable Terahertz Metamaterial Absorber with Broadband Absorption and Multiband Absorption. *Opt. Express* **2021**, *29*, 21551–21561. [CrossRef] [PubMed]
35. ElZein, B.; Elrashidi, A.; Dogheche, E.; Jabbour, G. Analyzing the Mechanism of Zinc Oxide Nanowires Bending and Bundling Induced by Electron Beam under Scanning Electron Microscope Using Numerical and Simulation Analysis. *Materials* **2022**, *15*, 5358. [CrossRef] [PubMed]
36. DeVore, J.R. Refractive Indices of Rutile and Sphalerite. *JOSA* **1951**, *41*, 416–419. [CrossRef]
37. Aspnes, D.E.; Studna, A.A. Dielectric Functions and Optical Parameters of Si, Ge, Gap, Gaas, Gasb, Inp, Inas, and Insb from 1.5 to 6.0 Ev. *Phys. Rev. B* **1983**, *27*, 985. [CrossRef]
38. Kaur, D.; Bharti, A.; Sharma, T.; Mahu, C. Dielectric Properties of ZnO-Based Nanocomposites and Their Potential Applications. *Int. J. Opt.* **2021**, *2021*, 995020. [CrossRef]
39. Elrashidi, A. Light Harvesting in Silicon Nanowires Solar Cells by Using Graphene Layer and Plasmonic Nanoparticles. *Appl. Sci.* **2022**, *12*, 2519. [CrossRef]
40. O'Hara, J.F.; Smirnova, E.; Azad, A.K.; Chen, H.-T.; Taylor, A.J. Effects of Microstructure Variations on Macroscopic Terahertz Metafilm Properties. *Act. Passiv. Electron. Compon.* **2007**, *2007*, 049691. [CrossRef]
41. Li, W.; Wu, T.; Wang, W.; Guan, J.; Zhai, P. Integrating Non-Planar Metamaterials with Magnetic Absorbing Materials to Yield Ultra-Broadband Microwave Hybrid Absorbers. *Appl. Phys. Lett.* **2014**, *104*, 22903. [CrossRef]
42. Elrashidi, A. Highly Sensitive Silicon Nitride Biomedical Sensor Using Plasmonic Grating and ZnO Layer. *Mater. Res. Express* **2020**, *7*, 75001. [CrossRef]
43. Zhou, Y.; Qin, Z.; Liang, Z.; Meng, D.; Xu, H.; Smith, D.R.; Liu, Y. Ultra-Broadband Metamaterial Absorbers from Long to Very Long Infrared Regime. *Light Sci. Appl.* **2021**, *10*, 1–12. [CrossRef] [PubMed]
44. Shi, Y.; Li, Y.C.; Hao, T.; Li, L.; Liang, C.-H. A Design of Ultra-Broadband Metamaterial Absorber. *Waves Random Complex Media* **2017**, *27*, 381–391. [CrossRef]
45. Zhang, C.; Yin, S.; Long, C.; Dong, B.W.; He, D.; Cheng, Q. Hybrid Metamaterial Absorber for Ultra-Low and Dual-Broadband Absorption. *Opt. Express* **2021**, *29*, 14078–14086. [CrossRef]
46. Liu, W.; Tian, J.; Yang, R.; Pei, W. Design of a Type of Broadband Metamaterial Absorber Based on Metal and Graphene. *Curr. Appl. Phys.* **2021**, *31*, 122–131. [CrossRef]
47. Cheng, Y.; Luo, H.; Chen, F. Broadband Metamaterial Microwave Absorber Based on Asymmetric Sectional Resonator Structures. *J. Appl. Phys.* **2020**, *127*, 214902. [CrossRef]
48. Thi Quynh Hoa, N.; Huu Lam, P.; Duy Tung, P. Wide-angle and Polarization-independent Broadband Microwave Metamaterial Absorber. *Microw. Opt. Technol. Lett.* **2017**, *59*, 1157–1161. [CrossRef]